Waveguide Bandpass Filters for Millimeter-Wave Radiometers

Furtula, V.; Zirath, H.; Salewski, Mirko

Published in:
Journal of Infrared, Millimeter and Terahertz Waves

Link to article, DOI:
10.1007/s10762-013-0013-4

Publication date:
2013

Noname manuscript No.
(will be inserted by the editor)

Waveguide Bandpass Filters for Millimeter-Wave Radiometers

Vedran Furtula · Herbert Zirath · Mirko Salewski

Received: date / Accepted: date

Abstract A fundamental requirement for most mm-wave heterodyne receivers is the rejection of the input image signal which is located close to the local oscillator frequency. For this purpose we use a bandpass filter, which for heterodyne receivers is also called an image rejection filter. In this paper we present a systematic approach to the design of a waveguide bandpass filter with a passband from 100 to 110 GHz and upper rejection bandwidth in the range from 113 to 145 GHz. We consider two non-tunable filter configurations: the first one is relatively selective with 11 sections (poles) whereas the second one is simpler with 5 sections. We used established design equations to propose an initial guess for the geometries of the filters, optimized the geometries, constructed the filters using two different milling methods, measured their transmission and reflection characteristics, and compared the measurements with numerical simulations. Measurements of both filters agree well with simulations in frequency response and rejection bandwidth. The insertion loss of the 11-pole filter is better than 10 dB and that of the 5-pole filter is better than 5 dB. The 11-pole filter has a sharper attenuation roll-off compared with the 5-pole filter. The upper out-of-band rejection is better than 40 dB up to 145 GHz for the 11-pole filter and up to 155 GHz for the 5-pole filter.

Keywords waveguide · millimeter waves · bandpass filter · fusion · diagnostics

Vedran Furtula and Herbert Zirath
Microwave Electronics Laboratory, Dept. of Microtechnology and Nanoscience
Chalmers University of Technology
Gothenburg, SWEDEN-41296
E-mail: furtula@chalmers.se, herbert.zirath@chalmers.se

Mirko Salewski
Association EURATOM - DTU
Technical University of Denmark
Dept. of Physics, Section for Plasma Physics and Fusion Energy
Risø Campus, Roskilde, DENMARK-4000
E-mail: msal@fysik.dtu.dk

1 Introduction

Bandpass filters are often used in millimeter wave receiver systems if not other components limit the passband width. They separate the spectral range of wanted signals from other radiation constituting noise. Usually, mm-wave receivers rely on the principle of heterodyne or beat reception: A mixer down-converts high-frequency signals to low-frequency signals since at lower frequency filtering is easier and the spectral resolution can be higher. A bandpass filter in the high-frequency branch of heterodyne detection systems has two functions: First, it limits the overall system bandwidth. Second, it eliminates the down-converted image signal to the same low-frequency band. In a typical mm-wave receiver a bandpass filter will introduce 2-5 dB insertion loss and thereby contribute to the system noise figure.

We find that a bandpass filter with a center frequency of 105 GHz and fractional bandwidth of 10% is suitable to remove the sideband noise during power measurements in W-band (75-110 GHz) and F-band (90-140 GHz). This filter could be used in systems where harmonic-producing components such as mixers and multipliers are built-in. Another field of application is in receivers sensitive to radiation coming from fusion plasmas, the so called total-power radiometers [1–5]. These receivers are often sensitive in the range from 50 GHz (V-band) to 170 GHz (F-band). Higher frequency bands are also of interest but the diagnostic solutions for these bands are technologically difficult and expensive. An

example of a receiver operating at 100-110 GHz is that of the collective Thomson scattering (CTS) diagnostic at ASDEX Upgrade [1,2,6–11]. It can detect spectral power densities of a few eV against the electron cyclotron emission (ECE) background on the order of 100 eV under presence of gyrotron stray radiation that is many orders of magnitude stronger than the signal to be detected. At ASDEX Upgrade there are also gyrotrons to heat the plasma at 140 GHz. It is therefore important that bandpass filters installed in this system have a high rejection up to at least 140 GHz [6,7]. Another type of diagnostic that uses bandpass filters with large fractional bandwidth is ECE spectroscopy where the objective is to determine the evolution of the electron temperature profile as a function of time covering the spectral range from 60 to about 800 GHz [3,12,13]. For example, the ECE diagnostics at ASDEX Upgrade detects radiation in a bandwidth of 20 GHz centered at 140 GHz [14].

Extensive literature exists on waveguide junctions, waveguide transitions, and waveguide filters [15–18], and we will use the findings and calculations from these references as initial steps towards final designs. Most available passive millimeter-wave components are fabricated using metallic waveguide structures but recent attempts have been done to design silicon micromachined D-band 3-pole and 5-pole bandpass filters [19].

In this paper we present two similar types of waveguide bandpass filters with a passband in the range from 100 to 110 GHz: one filter has 11 resonator sections (poles), and the other has 5 resonator sections. Both filters are fabricated using micromachined metallic waveguide structures. The 5-pole filter has wider rejection bandwidth compared with the 11-pole filter but due to the lower number of sections it is less selective in the attenuation roll-off region [15,20].

2 Analysis and Design Equations

The synthesis of filters in this article is based on Tchebyscheff factors with an odd number of sections. We do not use an even number of sections since it would require impedance transformation for the last stage of the filter [16, pp.95-104]. From Tchebyscheff's synthesis with an odd number of sections n, we have a symmetry in the filter that is illustrated in fig. 1: the first section on one side is identical to the first section on the other side; the second section on one side is identical to the second section on the other side and so forth. Hence the total number of different sections is $(n+1)/2$. Such a filter has $n+1$ window couplings, but likewise the first coupling on one side is identical to the first coupling on the other side etc. Hence there are $(n+1)/2$ different couplings.

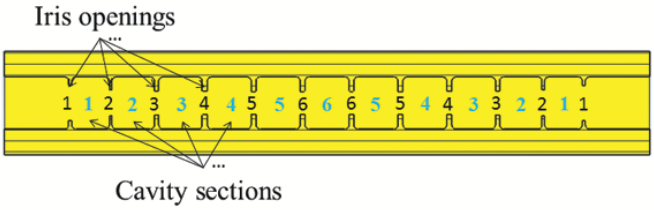

Fig. 1 Numbering of iris openings and cavity sections for an 11-pole filter.

In this paper we choose the principle of *direct coupling* as a technique to cascade resonant sections [17] where 1 section corresponds to 1 pole derived from Tchebyscheff's synthesis. In direct coupling technique much of the frequency sensitivity of the coupling sections is eliminated [17, p.258] and the filter structure becomes more compact. Therefore, we design the bandpass filter as cascade of $\sim \lambda_g/2$ sections connected with very thin couplings (window irises, see fig. 2(a)) which determine the width of the filter passband. The quantity λ_g is the guide wavelength for the fundamental TE_{10} mode, which in the case of an air-filled waveguide with uniform cross-section is

$$\lambda_g = \frac{\lambda_0}{\sqrt{\epsilon_r \mu_r - \left(\frac{\lambda_0}{\lambda_c}\right)^2}}, \tag{1}$$

where $\lambda_c = 2a$ is the cut-off wavelength, $\epsilon_r \mu_r = 1$ for the air-filled waveguide, and λ_0 is the wavelength in vacuum. The waveguide dimensions are set to $a = 2.032\ mm$ and $b = 1.016\ mm$ with the cut-off frequency at 73.84 GHz according to the WR-8 waveguide standard. As an alternative to the direct coupling technique, one can also choose the principle of *quarter-wavelength coupling*, where $\lambda_g/4$ sections [20, pp.468-476] are inserted between the poles. For the quarter-wavelength coupling the total number of resonant cavities (sections) will be increased to $2n-1$ where n is the number of poles.

Given the requirements for the filter, such as center frequency, passband bandwidth, and attenuation roll-off, we determine the number of required poles and calculate the section lengths and iris openings of the filter. Assuming Tchebyscheff's filter synthesis and 0.2 dB passband ripple from 100 to 110 GHz, we find that an 11-pole filter is adequate to satisfy an attenuation roll-off minimum of 60 dB, 2 GHz away from the band edges, i.e. 98 and 112 GHz. For the end discontinuities (no. 1 and 12 in tab. 1) we find the normalized iris susceptance

$\bar{b}_k$ to be [17, pp.290-294]

$$\bar{b}_k = \pm \left(\frac{\lambda_0}{\lambda_g}\right) \sqrt{\frac{2}{\pi} g_k \frac{f_0}{\Delta f_0}}, \tag{2}$$

where the plus-sign is reserved for capacitive irises and the minus-sign for inductive irises, and g_k are the Tchebyscheff factors for the k'th pole assuming $g_0 = g_{n+1} = 1$ for a filter with n poles. The quantity $f_0 = \sqrt{f_1 f_2} \approx 105$ GHz is the center frequency calculated using passband ripple edges f_1 and f_2. The quantity $\Delta f_0 = f_2 - f_1$ is the passband bandwidth. The filter geometry we use here requires inductive window irises and therefore $\bar{b}_k$ in eq. (2) is negative [18, p.184]. For the discontinuities between the sections, the iris susceptances $\bar{b}_{k,k+1}$ are dependent on the normalized impedances (Tchebyscheff factors) of the preceding resonator and the following resonator, so we get

$$\bar{b}_{k,k+1} = \pm \left(\frac{\lambda_0}{\lambda_g}\right)^2 \frac{2 f_0}{\pi \Delta f_0} \sqrt{g_k g_{k+1}}. \tag{3}$$

Using the principle of variational methods on the total stored electric and magnetic energy [15], it is possible to derive the iris susceptance $\bar{b}$ [18, p.165] from the geometrical configuration presented in fig. 2,

$$\bar{b} = -\frac{\lambda_g}{a} \cot^2 \frac{d\pi}{2a}, \tag{4}$$

where d is the width of the iris opening along the broad side of the waveguide. Since d is a design parameter we wish to calculate, we can rearrange eq. (4) as

$$d = \frac{2a}{\pi} \operatorname{arccot} \sqrt{-\bar{b} \frac{a}{\lambda_g}}, \tag{5}$$

where $\bar{b}$ represents susceptance for end discontinuities in eq. (2) or intersection discontinuities in eq. (3). The length of the resonant section l_k is found by the method of admittance matching across the iris

$$l_k = \frac{\lambda_g}{2\pi} \left(n\pi + \frac{1}{2} \arctan \frac{2}{\bar{b}_{k,k+1}} + \frac{1}{2} \arctan \frac{2}{\bar{b}_{k+1,k+2}} \right) \tag{6}$$

where $\bar{b}_{k,k+1}$ and $\bar{b}_{k+1,k+2}$ are the two iris susceptances on each side of the section calculated using eq. (3). The loaded quality factor Q_{Lk} is calculated for each section (cavity) k using the expression for the susceptance $\bar{b}_k$ presented in eq. (2)

$$Q_{Lk} \approx \frac{\pi}{4} \bar{b}_k^2 \left(\frac{\lambda_{g0}}{\lambda_0}\right)^2. \tag{7}$$

Using eqs. (5) and (6) we can now determine the lengths of the cavity sections l_k and widths of the iris openings d_k, respectively.

Section	l_k [mm]	Q_{Lk}-factor	Iris	d_k [mm]
1 / 11	1.6457	7.3	1 / 12	0.9872
2 / 10	1.7828	7.3	2 / 11	0.7445
3 / 9	1.8143	12.2	3 / 10	0.6710
4 / 8	1.8204	8.1	4 / 9	0.6574
5 / 7	1.8224	12.6	5 / 8	0.6529
6	1.8229	8.2	6 / 7	0.6513

Table 1 Initial design parameters and loaded quality factors Q_{Lk} for the 11-pole bandpass filter.

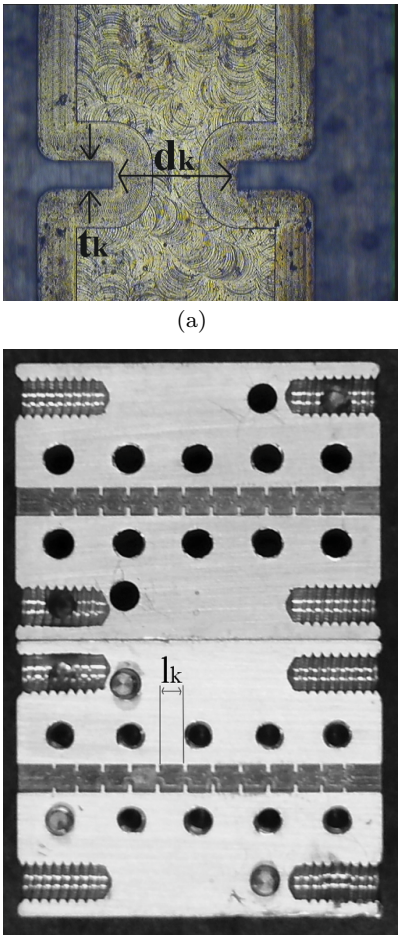

(a)

(b)

Fig. 2 (a) Photograph of an iris coupler with thickness $t_k \approx 0.1$ mm and opening $d_k \approx 1$ mm; (b) The two milled symmetrical parts of the 11-pole bandpass filter.

3 11-Pole Bandpass Filter - Simulations and Measurements

The design parameters from tab. 1 are used to model a waveguide filter in the 3D electromagnetic simulation environment CST [21]. The S-parameter simulated and presented in this work are calculated using the time domain solver with discrete waveguide ports using more than two million meshcells. However, in the intermediate steps during scaling and optimization we

Section	l_k [mm]	Iris	t_k [mm]	d_k [mm]
1 / 11	1.4637	1 / 12	0.119	1.3714
2 / 10	1.6457	2 / 11	0.101	1.00
3 / 9	1.6881	3 / 10	0.1665	0.9319
4 / 8	1.6968	4 / 9	0.2037	0.9159
5 / 7	1.712	5 / 8	0.195	0.8878
6	1.7145	6 / 7	0.1853	0.8924

Table 2 Optimized section lengths l_k, iris openings d_k, and iris thicknesses t_k for the 11-pole bandpass filter.

have used the frequency domain solver with approximately 400,000 meshcells. The waveguide material is brass with a conductivity of $1.6 \cdot 10^7$ S/m. The waveguide sections with 270° edges are blended with a radius of 0.15 mm (Ø 0.3 mm drill). The filter is divided into two symmetrical parts, i.e. H-plane cut at the position $b/2$ where b is the short side of the waveguide. The two filter sides are connected and kept tight together using 10 (Ø 2 mm) flat head screws. We could also have used an E-plane cut across the position $a/2$ but the drilling depth would have been twice as large as for the H-plane cut. Due to mechanical tolerances this would imply a drill of minimum Ø 0.5 mm making blended edges larger and thereby lowering the Q-factor of the resonating cavities.

The initial simulation results do not fit the passband bandwidth of the filter, so we choose to scale the section lengths l_k and the iris openings d_k in such a way that both the center frequency and the bandwidth match the S-parameter requirements. By scaling the section lengths l_k it is possible to move the filter passband up or down in frequency. By scaling the iris openings d_k it is possible to expand or contract the bandwidth. It turns out that the filter should be scaled by the factors $\Delta_{l_k} = 0.975$ and $\Delta_{d_k} = 1.198$, i.e. the section lengths should be shortened by 2.5% and the iris openings should be widened by 19.8% in order to match the target center frequency and bandwidth.

As a last step we choose to optimize the section lengths l_k, the iris openings d_k, and the iris thicknesses t_k in order to find the optimum geometry for the filter so that we can meet the requirements set by Tchebyscheff's synthesis. The values determined by the optimization are found in tab. 2. By optimizing the geometry with CST, we can determine if there is a significant improvement in the S-parameters compared with the S-parameters from the scaled geometry. The method of optimization used is *Trust region framework* where we optimized at most 3 parameters at a time from the total number of 18 optimization parameters. The optimized values for l_k and d_k differ less than 10% and 16%, respectively, from the corresponding scaled values, while the optimized iris thicknesses t_k are scattered in the range from 0.1 to 0.2 mm.

The filter performance was measured using the vector network analyzer (VNA) HP8510C with the waveguide interface where the ports were calibrated using the TRL technique; T = thru (waveguide ports directly connected), R = reflect (short at port 1 and port 2), L = line ($\lambda/4$ waveguide section between the ports). The VNA intermediate frequency (IF) bandwidth was chosen to be 1 kHz, and the number of measurement points was 401. The filter S-parameters were very sensitive to the torque applied to the connecting screws, where a single loose screw could result in additional passband loss in the range from 0.5 to 1 dB.

The simulated and measured S-parameters for the filter transmission loss and input/output matching are presented in fig. 3. During the simulation we also assume that $S_{11} = S_{22}$ since we have three symmetrical planes in the filter geometry. The measured insertion loss in the passband is 5 to 10 dB worse than was predicted in the simulations. Furthermore, the insertion loss becomes larger ($\approx$ 10 dB) for the frequencies around 100 GHz in the measurements whereas the simulation predicts approximately constant attenuation in the passband. One possible explanation for the high loss is the H-plane cut that introduces a discontinuity in the waveguide which disturbs the flow of the surface currents induced by the **H**-field. The measured return losses at the input and output ports which correspond to S_{11} and S_{22} in fig. 3, respectively, are lower than 15 dB showing good agreement with the simulations. We notice a clear difference between S_{11} and S_{22}, particularly at frequencies around 100 GHz, which indicates that we do not have a complete symmetry in the fabricated filter or that the material properties of the brass vary along the filter. The steepness of the attenuation roll-off match the simulations reasonably well which indicates that the simulated loaded Q-factors, Q_{Lk} in eq. (7), are in agreement with the conductor loss in brass.

Measured and simulated transmission characteristics in the out-of-band frequency range 140-220 GHz (G-band) are shown in fig. 4. The measurements in the G-band are accomplished using a programmable network analyzer (PNA) E8361A attached to a pair of OML [22] extenders with WR-05 waveguide flanges. The simulations in fig. 4 show appearance of a secondary passband with low insertion loss in the range from 150 to 177 GHz, which is however not clearly observed in the measurements. Eigenmode analysis shows that the 1'st higher order mode is found at approximately 150 GHz for the smallest sections, which are no. 1 and no. 11, and similarly the 1'st higher order

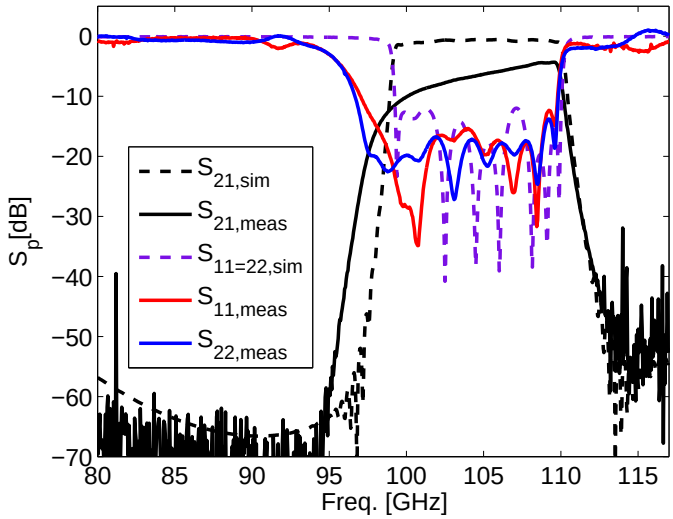

Fig. 3 Simulated and measured primary-band transmission characteristics (S_{21}), input matching (S_{11}) and output matching (S_{22}) of the 11-pole bandpass filter.

mode is found at approximately 175 GHz for the largest section, which is no. 6. This makes the 11-pole filter suitable for frequency operations in the range from 112 to 145 GHz with rejection better than 40 dB.

4 5-Pole Bandpass Filter - Simulations and Measurements

The measured S-parameters of the 11-pole filter agree relatively well with the simulations considering the frequency response. However, the insertion loss in the passband is somewhat higher than we expected. A way to reduce the insertion loss is to reduce the number of sections, and so we made a similar filter but with 5 sections, i.e. a 5-pole bandpass filter. Three major changes are introduced in the 5-pole filter compared with the 11-pole filter. Firstly, we choose to fix the window iris thicknesses to 0.1 mm as shown in fig. 5(a). Secondly, the 270° edges are blended with radius of 0.25 mm (Ø 0.5 mm drill) such that no change of the milling drill is necessary during the production (see fig. 5(a)). This will simplify the milling process but will reduce the Q-factors of the cavity sections slightly. Thirdly, the cavity sections are milled on one half of the filter leaving the other half blank (see fig. 5(b)), which reduces tolerances of the filter geometry. The two unsymmetrical filter sides are kept tight together with 4 socket head screws (Ø 3 mm). The fundamental waveguide dimensions are set to $a = 2.54$ mm and $b = 1.27$ mm so that the cut-off frequency at 59 GHz complies with WR-10 waveguide standard. The waveguide dimensions a and b are increased, compared with those for the 11-pole filter, so that they match the interface of the measurement set-up.

Section	l_k [mm]	Q_{Lk}-factor	Iris	d_k [mm]
1 / 5	1.4560	7.0	1 / 5	1.0328
2 / 4	1.5739	7.0	2 / 4	0.7138
3	1.5917	11.4	3	0.6417

Table 3 Initial values for l_k and d_k and loaded quality factors Q_{Lk} for the 5-pole bandpass filter.

Section	l_k [mm]	Iris	t_k [mm]	d_k [mm]
1 / 5	1.435	1 / 6	0.1	1.0737
2 / 4	1.551	2 / 5	0.1	0.8086
3	1.566	3 / 4	0.1	0.749

Table 4 Optimized section lengths l_k, iris openings d_k, and iris thicknesses t_k (fixed) for the 5-pole bandpass filter.

Assuming Tchebyscheff's synthesis and 0.2 dB passband ripple from 100 to 110 GHz, we find that a 5-pole filter satisfies an attenuation roll-off minimum of 27 dB, 3 GHz away from the band edges, i.e. 97 and 113 GHz. From eqs. (5) and (6) we can determine the initial lengths of the cavity sections l_k and the widths of the iris openings d_k. The results are shown in tab. 3.

As in the case of the 11-pole filter, the initial simulations do not agree with the required passband bandwidth, and so we choose to scale the section lengths l_k and the iris openings d_k. Hereby, the simulated filter is multiplied by the factors $\Delta_{l_k} = 0.984$ and $\Delta_{d_k} = 1.158$ implying that the section lengths l_k should be shortened by 1.6% and the iris openings d_k should be widened by 15.8% in order to match the required passband and center frequency.

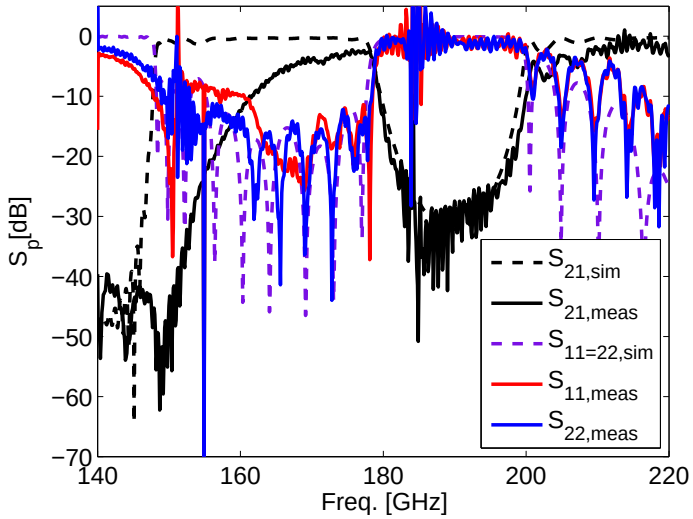

Fig. 4 Simulated and measured out-of-band transmission characteristics (S_{21}), input matching (S_{11}) and output matching (S_{22}) of the 11-pole bandpass filter.

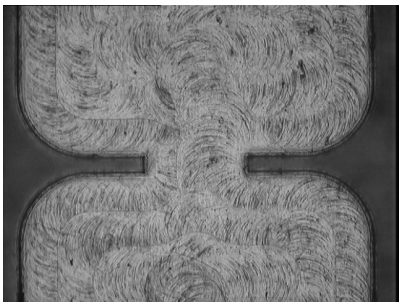

(a)

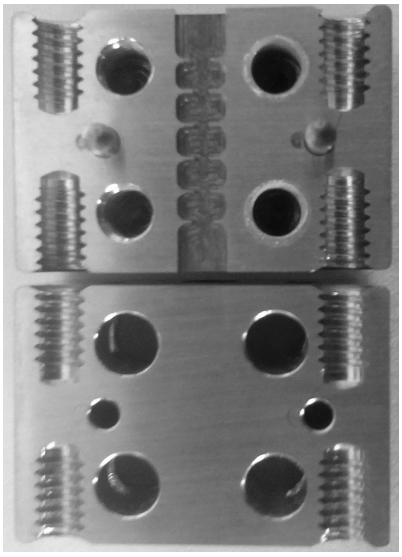

(b)

Fig. 5 The two halves of the filter block. The cavity sections are milled in one of the two halves using iris couplers with fixed thickness $t_k = 0.1$ mm and iris openings d_k in the range from 0.7 to 1 mm (a), while the other half of the block is left blank (b).

Thereafter we optimize the geometry in the same way as for the 11-pole filter. The optimized values for l_k and d_k shown in tab. 4 are within 0.15% and 11.5% of the scaled values, respectively. We have observed that the optimized cavity lengths are almost unchanged from the scaled values, while iris openings have more significant changes. Especially, the first and the last optimized iris opening (no. 1 and no. 6) are the most critical. The iris thicknesses t_k are not optimized but kept constant at 0.1 mm.

The simulated and measured S-parameters are presented in fig. 6. The measured passband insertion loss is better than 5 dB, but it has a slight slope compared with the simulations where the insertion loss is a flat function of frequency. The filter return losses at the input port and the output port (S_{11} and S_{22}, respectively) are better than 8 dB and match reasonably well with the simulated cavity resonances. We also notice less difference between S_{11} and S_{22} compared with the case of the 11-pole filter, which indicates that we have achieved a relatively good symmetry in the fabricated 5-pole filter.

The measured and simulated transmission in the out-of-band frequency range is presented in fig. 7. The simulations and measurements show appearance of a secondary passband in the range from 166 to 190 GHz. Eigenmode analysis shows that the 1'st higher order mode after the fundamental is found at approximately 165 GHz. Hereby, the 5-pole bandpass filter is suitable for frequency operations in the range from 115 to 155 GHz with a rejection better than 40 dB.

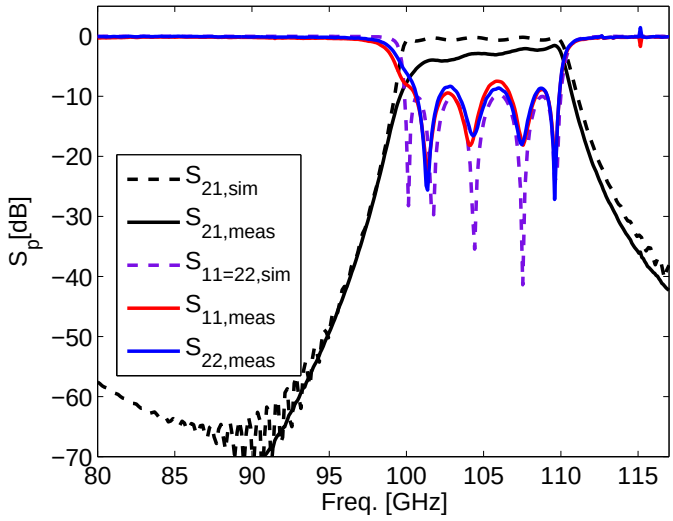

Fig. 6 Simulated and measured primary-band transmission characteristics (S_{21}), input matching (S_{11}) and output matching (S_{22}) of the 5-pole bandpass filter.

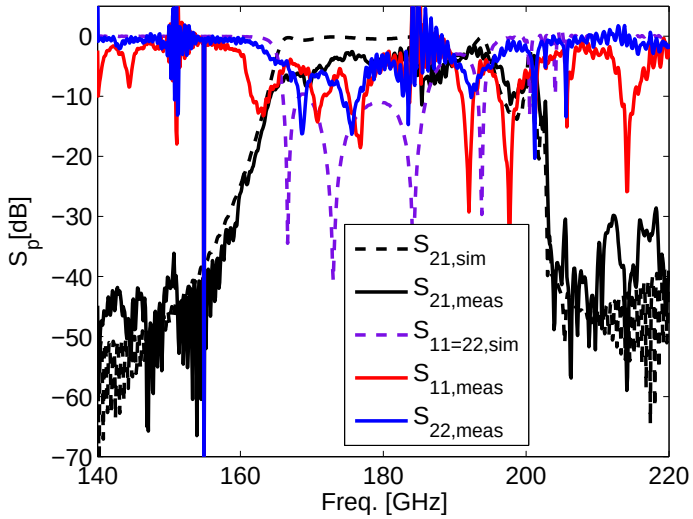

Fig. 7 Simulated and measured out-of-band transmission characteristics (S_{21}), input matching (S_{11}) and output matching (S_{22}) of the 5-pole bandpass filter.

5 Conclusions

We have fabricated two bandpass filters with a passband from 100 to 110 GHz, one with 11 sections and one with 5 sections. We compare measured S-parameters with simulated ones. Measurements of the 11-pole filter agree relatively well with simulations in frequency response and rejection bandwidth, and the insertion loss is better than 10 dB. For the 5-pole filter, the simulated frequency response and the rejection bandwidth match the measurements very well. We find that the insertion loss is better than 5 dB.

The 5-pole filter has lower insertion loss than the 11-pole filter, but its attenuation roll-off is not as sharp as that of the 11-pole filter. The 5-pole filter shows very good out-of-band rejection properties up to 155 GHz, while the 11-pole filter has good out-of-band rejection up to 145 GHz. Both filters are simulated using values derived from the design eqs. (2)-(6), where we noticed that the simulated passband was narrower than expected. Therefore we scale the sections lengths l_k and iris openings d_k with factors Δ_{l_k} and Δ_{d_k}, respectively. The scaled filters provide S-parameters that are relatively close to the requirements derived from Tchebyscheff's synthesis. Further improvements of the filter

response are possible by optimizing section lengths l_k and iris openings d_k. The optimized S-parameters differ from the scaled ones by less that 11.5% for the 5-pole filter and less than 19.8% for the 11-pole filter. It turns out that it is necessary to optimize the first (and last) iris opening and the first (and last) section after scaling all sections and iris openings. We can summarize a recipe for waveguide bandpass filter design as follows: Choose an odd number of sections for your design that will meet your passband bandwidth and attenuation roll-off requirements. Find the corresponding Tchebyscheff factors. Use eqs. (2)-(6) to determine an initial geometry for your filter and fix the iris thickness t_k to a relatively small value ($b \gg t_k$). Simulate your filter and then determine scaling factors Δ_{l_k} and Δ_{d_k} so that passband requirements are met. Finally optimize the first (and last) section lengths l_1 (l_n) as well as the first (and last) iris opening d_1 (d_{n+1}).

Acknowledgment

The authors would like to thank Carl-Magnus Kihlman for the fabrication of filters.

References

1. V. FURTULA *et al.*, "Design and performance of the collective Thomson scattering receiver at ASDEX Upgrade," *Rev. Sci. Instrum.*, vol. 83, p. 013507, 2012.
2. V. FURTULA *et al.*, "Performance measurements of the collective Thomson scattering receiver at ASDEX Upgrade," *J. of Instr.*, vol. 7, pp. 1748–0221/7, 2012.
3. H. J. HARTFUSS, T. GEIST, and M. HIRSCH, "Heterodyne methods in millimetre wave plasma diagnostics with applications to ECE, interferometry and reflectometry," *Plasma Phys. Control. Fusion*, vol. 39, no. 11, pp. 1693–1769, 1997.
4. J. MONTEJO-GARAI *et al.*, "Synthesis and design of waveguide band-stop filters without out-of-band spurious responses for plasma diagnosis," *Fusion Eng. Des.*, vol. 87, no. 9, pp. 1662–1666, 2012.
5. M. SALEWSKI *et al.*, "Investigation of first mirror heating for the CTS diagnostic in ITER," *Rev. Sci. Instrum.*, vol. 79, p. 10E729, 2008.
6. V. FURTULA *et al.*, "Broadband notch filter design for millimeter-wave plasma diagnostics," *Rev. Sci. Instrum.*, vol. 81, p. 10D913, 2010.
7. F. MEO *et al.*, "Commissioning activities and first results from the collective Thomson scattering diagnostic on ASDEX Upgrade," *Rev. Sci. Instrum.*, vol. 79, p. 10E501, 2008.
8. F. MEO *et al.*, "First results and analysis of collective Thomson scattering (CTS) fast ion distribution measurements on ASDEX Upgrade," *J. Phys.: Conf. Series*, vol. 227, no. 1, p. 012010, 2010.
9. M. SALEWSKI *et al.*, "Comparison of fast ion collective Thomson scattering measurements at ASDEX Upgrade with numerical simulations," *Nucl. Fusion*, vol. 50, no. 3, p. 035012, 2010.
10. M. SALEWSKI *et al.*, "On velocity space interrogation regions of fast-ion collective Thomson scattering at ITER," *Nucl. Fusion*, vol. 51, no. 8, p. 083014, 2011.
11. M. SALEWSKI *et al.*, "Tomography of fast-ion velocity-space distributions from synthetic CTS and FIDA measurements," *Nucl. Fusion*, vol. 52, no. 10, p. 103008, 2012.
12. E. de la LUNA and J. contributors, "Physics of ECE temperature measurements and prospects for ITER," in *An International Conference on BURNING PLASMA DIAGNOSTICS*, pp. 63–72, American Institute of Physics, September 2007.
13. G. VAYAKIS *et al.*, "ECE diagnostics for RTO/RC ITER," *Fusion Eng. Des.*, vol. 53, no. 1-4, pp. 221–227, 2001.
14. W. A. BONGERS *et al.*, "Commissioning of inline ECE system within waveguide based ECRH transmission systems on ASDEX Upgrade," *EPJ Web of Conferences*, vol. 32, no. 03006, pp. p.1–p.6, 2012.
15. N. MARCUVITZ, *Waveguide Handbook*. Brooklyn, N.Y.: Peter Peregrinus Ltd., London, UK, 1986.
16. G. MATTHAEI, L. YOUNG, and E. M. T. JONES, *Microwave Filters, Impedance-Matching Networks, and Coupling Structures*. 685 Canton Street, Norwood, MA 02062: Artech House, 1980.
17. J. L. ALTMAN, *Microwave Circuits*. D. Van Nostrand Company, Inc.: Artech House, 1964.
18. C. G. MONTGOMERY, R. H. DICKE, and E. M. PURCELL, *Principles Of Microwave Circuits*. The Maple Press Company, York, PA: McGraw-Hill Book Copmany, Inc., 1948.
19. X. H. ZHAO *et al.*, "D-band micromachined silicon rectangular waveguide filter," *IEEE Microwave and Wireless Components Lett.*, vol. 22, no. 5, pp. 230–232, 2012.
20. P. A. RIZZI, *Microwave Engineering - Passive Circuits*. Englewood Cliffs, New Jersey 07632: Prentice-Hall, Inc., 1988.
21. Computer Simulation Technology (CST), "Microwave studio," 2012.
22. OML Inc., "V05VNA-T/R," 2008.